THE ASTROPHYSICAL JOURNAL, 292:628–639, 1985 May 15

RADIO AND INFRARED OBSERVATIONS OF OH/IR STARS AT THE TANGENTIAL POINT AND NEAR THE GALACTIC CENTER

B. BAUD,[1,2] ANNEILA I. SARGENT,[3] M. W. WERNER,[4] AND A. F. BENTLEY[5]
Received 1984 October 10; accepted 1984 November 30

ABSTRACT

We have determined accurate radio positions and subsequently made simultaneous infrared and OH radio measurements of a sample of OH/IR stars near the tangential point and in the galactic center. Intrinsic physical parameters of the stars and their dust shells, as well as the maser luminosities, have been determined. They are consistent with the stars being at the top of the asymptotic giant branch; the dense circumstellar shells suggest that they are evolving rapidly through a phase of high mass loss.

Our sample comprises stars of widely different masses and luminosities; it is shown that the OH luminosity is strongly dependent on the degree of reddening of the circumstellar shell, i.e., on the stellar mass-loss rate. In addition, a quantitative relation between the OH luminosity and the optical depth in the 10 μm silicate feature has been determined for the sample. This predicts the observed time variations in the strength of the silicate feature with time-variable stellar luminosity. While the stars in the galactic center sample are systematically less luminous than those at the tangential point, the derived relations apply equally to each group.

Subject headings: infrared: sources — masers — stars: circumstellar shells — stars: late-type

I. INTRODUCTION

Combined infrared and OH observations are essential to understanding the nature of OH/IR stars, the properties of their circumstellar envelopes, and the OH maser pump mechanism (cf. Werner *et al* 1980; Herman 1983). These cool, variable stars, typical of the Asymptotic Giant Branch (AGB) in the H-R diagram, have generally been found through OH radio surveys (e.g., Johansson *et al.* 1977; Bowers 1978; Baud *et al.* 1979*a*, *b*), and many are strong infrared sources with thick circumstellar dust shells. Since their OH maser emission can be detected at large distances from the Sun, OH/IR stars can be used to study the population distribution, kinematics, and evolution of stars on a galactic scale (cf. Baud *et al.* 1981, hereinafter BHMW). Moreover, these objects constitute a unique tool for examining stellar evolution at the tip of the AGB, a region of the H-R diagram which is poorly understood theoretically and where circumstellar obscuration often precludes optical observations. From infrared observations of these objects, the luminosities of the underlying stars and the masses of the circumstellar envelopes may be derived, while the double-peaked OH emission-line profiles yield both the stellar radial velocity v and the circumstellar shell expansion velocity v_e; the latter quantity is statistically related to the main-sequence mass (BHMW). Comparison of the visible, low OH luminosity Mira variables with the optically obscured, but strong OH emitting, OH/IR stars indicates that OH luminosity is related to the stellar mass-loss rate, and it has been suggested (Baud and Habing 1983, hereinafter BH; Jones *et al.* 1983) that such OH/IR stars represent the end point of the Mira evolution on the AGB; their large mass-loss rates imply that some may be evolving toward a planetary nebula stage.

In this paper we present unambiguous infrared identifications of a sample of OH/IR stars in the galactic disk and in the vicinity of the galactic center. Simultaneous OH and broad-band infrared photometric measurements allow us to derive quantitative relations between the infrared and OH fluxes and the properties of the circumstellar shells, providing observational evidence that these stars represent an evolutionary sequence of increasing mass-loss rate. Using these relations, the observed time variations of the silicate absorption feature with changing bolometric luminosity in OH/IR stars can be explained. In addition, it appears that the ratio of the OH flux to the number of pump photons is not constant (e.g., Elitzur, Goldreich, and Scoville 1976) but is also a function of the mass-loss rate.

II. OBSERVATIONS

a) *The Sample*

A recurrent problem in determining the physical properties of OH/IR objects is the uncertainty and ambiguity in their distances, usually derived kinematically from the observed radial velocities. Most OH/IR stars have been discovered in flux-limited radio surveys, so that the near-kinematic distance is a plausible choice (cf. Jones, Hyland, and Gatley 1983), but, since the velocity dispersions are typically 10–30 km s^{-1} (BHMW), the distance uncertainties are large. For example, the near-kinematic distance of OH 26.5 + 0.6 is 1.8 kpc. A more reliable value of 1 kpc, resulting in a significantly lower estimate for the luminosity, has been derived using the observed angular size and the light travel time through the shell (Herman 1983).

The present study includes stars in the galactic plane whose high radial velocities indicate that they are at the tangential point—the position along the line of sight closest to the galactic center—and stars near the galactic center itself. For both groups the distance uncertainties are relatively small. The tangential sample was selected from the homogeneous list of BHMW, which is based on systematic OH surveys of the northern hemisphere (Johannsson *et al.* 1977; Bowers 1978; Baud *et al.* 1979*a*). It consists of (1) all stars with radial velo-

[1] Dept. of Space Research, Groningen, The Netherlands.
[2] Radio Astronomy Lab., University of California, Berkeley.
[3] Owens Valley Radio Observatory, California Institute of Technology, Pasadena.
[4] NASA/Ames Research Center, Moffett Field, California.
[5] Dept. of Natural Sciences, Eastern Montana College, Billings.

cities v larger than the maximum velocity v_{max} allowed by circular rotation (cf. Burton and Gordon 1978), and (2) stars with $v > (v_{max} - 10)$ km s^{-1} in cases where $v_e > 15$ km s^{-1}. Stars in the first group are assumed to be at the tangential point; excess velocities presumably reflect random motions. Although some distance ambiguity exists for the second group, the velocity dispersion of these stars is small (~ 10 km s^{-1}; BHMW), and they are probably within 25% of the tangential point.

The galactic center sample was chosen (1) from stars within a degree (170 pc) of the galactic center, with $|v| > 100$ km s^{-1} (Habing *et al.* 1983) and (2) for $l > 1°$, from a survey along the galactic plane (Olnon *et al.* 1981; Baud *et al.* 1979*b*). The first group are members of the galactic bulge population (e.g., Olnon *et al.* 1981), where the density of OH/IR stars is strongly enhanced. The latter are probably foreground objects and members of the galactic disk population (see appendix A).

The distribution of v_e in both samples is very similar to that for all OH/IR stars in the Galaxy (e.g., BHMW), as is the distribution in galactic latitude and longitude. However, since their average distance is large, these stars represent the high-luminosity tail of the OH luminosity distribution; L_{OH} ranges from 1 Jy kpc^2 for the nearby OH-emitting Miras to 1000 Jy kpc^2 for the brightest and most distant OH/IR stars (cf. Nguyen-Q-Rieu *et al.* 1979; BH), but for the samples here it is typically larger than 100 Jy kpc^2. Nevertheless, the number of stars in both samples increases steeply with decreasing OH luminosity (see Tables 1 and 2), which is consistent with the OH luminosity distribution found for all OH/IR stars (cf. BHMW). Most conclusions drawn from the present sample may therefore be extended to the majority of OH/IR stars.

b) Accurate Radio Positions and OH *Fluxes*

Since the OH objects in our sample lie within a degree of the galactic plane, and since single-dish OH measurements lead to positional uncertainties of $\pm 15''$ to $\pm 5'$, confusion with K and M giants along the line of sight can be a serious problem in identifying their near-infrared counterparts (cf. Jones *et al.* 1981, 1982). Interferometric observations of the 1612 MHz OH maser emission were therefore carried out to determine more accurate ($\pm 1''$) radio positions. The need for such positional accuracy is emphasized by the fact that two stars common to this sample and to that of Jones, Hyland, and Gatley (1983) appear to have been misidentified by these authors (see below).

1612 MHz OH observations of the tangential sample were made on two consecutive days in 1980 July with the Very Large Array (VLA) spectral line system of the National Radio Astronomy Observatory.[6] Observations were made with nine telescopes in a hybrid configuration and with baselines ranging from 0.3 to 3.4 km; the synthesized beam was typically $12'' \times 7''.5$. The instantaneous bandwidth of 780 kHz was divided among 128 autocorrelation channels, each 6.1 kHz wide (1.1 km s^{-1}). The instrumental phase and bandpass were calibrated using the unresolved continuum source 1741−038 (1.43 Jy based on 13.83 Jy for 3C 286 at 1612 MHz) and 3C 286 respectively.

Positions were determined from high-resolution maps of the high- and low-velocity components of the line profiles. In all cases, emission from the two components appeared unresolved and coincident within the uncertainties of the measurements. The results are listed in Table 1 in order of increasing galactic longitude; column (1) contains the source name and columns (2), (3), (4), and (5) the positions and 3 σ uncertainties in R.A. and Decl. respectively. Although stars from both this and the galactic-center sample are in some cases displaced by 0°.1 or more from the single-dish positions, the old source names have

[6] NRAO is operated by Associated Universities, Inc., under contract to the National Science Foundation.

TABLE 1

OH/IR STARS AT THE TANGENTIAL POINT: ACCURATE RADIO POSITIONS, VELOCITIES, AND PEAK OH FLUX DENSITIES

Name (1)	R.A. (1950) (2)	3 σ (3)	Decl. (1950) (4)	3 σ (5)	LV (km s^{-1}) (6)	HV (km s^{-1}) (7)	S_{LV}[a] (Jy) (8)	S_{HV}[a] (Jy) (9)	1 σ (Jy) (10)
OH 10.9+1.5	18^{h}00^{m}42^s.55	±1″.1	−18°41′18″.4	±1″.2	120.0	144.5	2.61	1.05	0.13
OH 17.2−1.1	18 23 19.55	±0.5	−14 30 08.0	±0.5	158.4	183.3	1.85	3.53	0.13
OH 18.2+0.5	18 19 07.21	±0.3	−12 56 50.2	±0.9	113.9	137.7	1.42	1.96	0.12
OH 18.5+1.4	18 16 47.37	±0.3	−12 09 27.8	±0.9	165.7	187.0	8.45	5.50	0.20
OH 20.7+0.1	18 25 44.32	±0.3	−10 52 51.1	±0.9	117.9	154.6	10.8	6.1	0.6
OH 21.5+0.5	18 25 45.49	±0.6	−10 00 12.4	±0.8	97.8	134.0	25.1	34.1	0.6
OH 24.7−0.1	18 34 03.61	±0.5	−07 20 52.3	±1.1	109.8	142.8	4.8	<1.5	0.5
OH 25.1−0.3	18 35 33.36	±0.6	−07 12 34.9	±1.4	130.0	154.8	7.44	6.60	0.25
OH 27.0−0.4	18 39 21.93	±0.6	−05 24 02.8	±1.1	87.3	116.4	3.71	8.02	0.24
OH 27.2+0.2	18 37 36.72	±0.8	−05 05 28.4	±0.8	72.6	111.4	2.1	2.2	0.3
OH 27.5−0.9	18 42 01.90	±0.6	−05 12 25.5	±0.6	93.0	120.0	7.03	6.11	0.25
OH 27.8−1.5	18 44 57.97	±0.8	−05 14 27.3	±0.9	70.1	100.5	2.27	2.79	0.16
OH 28.5−0.0	18 40 47.45	±0.6	−03 58 57.6	±0.8	93.9	120.6	11.85	11.41	0.24
OH 29.4−0.8	18 45 12.24	±0.4	−03 32 53.2	±1.4	113.6	137.3	10.35	5.81	0.27
OH 30.1−0.7	18 46 04.91	±0.3	−02 53 54.1	±0.8	78.4	119.0	57.2	59.6	0.4
OH 31.0−0.2	18 46 07.15	±0.8	−01 51 56.5	±1.1	111.4	140.1	5.22	6.56	0.37
OH 32.0−0.5	18 48 51.21	±0.8	−01 07 29.3	±0.6	55.0	96.0	8.3	5.1	0.4
OH 32.1+0.9	18 44 04.62	±0.8	−00 20 29.9	±0.6	124.7	149.3	2.36	3.77	0.17
OH 34.9+0.8	18 49 43.87	±1.1	+02 00 08.0	±0.7	54.0	82.9	2.39	3.10	0.11
OH 36.4+0.3 A	18 54 01.52	±0.6	+03 16 08.2	±0.6	83.5	121.1	4.88	2.76	0.19
OH 36.4+0.3 B	18 53 57.61	...	+03 13 21.1	...	...	...	...	...	...
OH 36.4+0.3 C	18 54 07.15	...	+03 14 02.1	...	...	...	...	...	...
OH 37.1−0.8	18 59 36.22	±0.8	+03 15 53.3	±1.1	75.0	101.5	14.41	20.32	0.47
OH 37.7−1.4	19 02 40.07	±0.3	+03 36 23.4	±0.6	100.0	119.9	2.32	0.47	0.16
OH 39.9−0.0	19 01 42.93	±0.6	+06 08 45.0	±0.8	133.7	163.0	3.6	6.2	0.4

[a] 1612 OH flux density at the time of the infrared observations; spectral resolution is 4.9 kHz.

TABLE 2

OH/IR STARS IN THE GALACTIC CENTER REGION: ACCURATE RADIO POSITIONS, VELOCITIES, AND PEAK OH FLUX DENSITIES

Name (1)	R.A. (1950)[a] (2)	Decl. (1950)[a] (3)	LV (km s^{-1}) (4)	HV (km s^{-1}) (5)	S_{LV}[b] (Jy) (6)	S_{HV}[b] (Jy) (7)
OH 359.1+1.1	17^{h}35^{m}56^s.98	−29°02′24″.8	−146.5	−128	2.3	2.8
OH 359.2+0.2	17 39 55.33	−29 29 36.1	−150	−121	0.9	2.0
OH 359.4+0.1	17 40 34.13	−29 24 59.5	−199	−223.5	0.8	2.2
OH 0.2+0.0	17 42 45.49	−28 44 10.0	+145	+174	1.1	0.7
OH 0.3−0.2	17 43 56.64	−28 43 41.2	−356	−327	2.3	1.9
OH 0.5−0.2	17 44 14.94	−28 35 31.8	+130	+153.5	0.9	1.5
OH 1.08+0.4	17 43 35.37	−27 48 47.2	−142	−108	<0.6	<0.6
OH 1.1−0.8	17 48 16.88	−28 24 52.7	−9	+30	20.6	24.5
OH 1.5−0.1	17 46 12.10	−27 41 00.8	−141.5	−114.5	2.7	5.1
OH 1.7−0.0	17 46 53.55	−27 24 10.0	−105	−134	0.8	3.5
OH 2.6−0.4	17 50 11.14	−26 56 01.5	−27	+18.5	13.3	14.2
OH 4.0+0.9	17 48 17.90	−25 01 08.7	+59	+88	1.3	1.0
OH 5.0−0.4	17 54 32.21	−25 12 42.6	−100	−146	1.8	2.5
OH 9.0−0.1	18 03 09.13	−21 14 02.4	−64	−33	<0.9	<0.9
OH 9.6+0.5	18 02 10.19	−20 22 30.6	−49	−76	2.0	3.5
OH 12.8−0.9	18 13 53.45	−18 16 08.9	−67	−44	9.7	2.3
OH 12.8+0.3	18 09 23.09	−17 43 48.1	+125	+152	<1.0	<1.0
OH 14.8+0.2	18 13 48.70	−16 05 15.0	+109	+133	<1.0	<1.0

[a] 3 σ uncertainties in R.A. = ±0″.3 and in Decl. = ±0″.9.

[b] 1612 MHz OH flux density on 1981 Aug 27–Sep 1; upper limits are 3 σ; spectral resolution is 4.9 kHz; 3 σ uncertainty is ± 0.2 Jy.

been adopted for consistency with other published work. Limited UV coverage for OH 36.4+0.3 resulted in some uncertainty; position A is the most likely but two less plausible positions (B and C) are also given. The positions of OH 37.7−1.4, observed on both days, agreed within 0″.2, confirming the accuracy of the measurements. Comparison with more recent VLA observations of some of the stars (Herman 1983) further strengthens our confidence in the results. For OH 20.7 and OH 31.0 the near-infrared positions listed by Jones, Hyland, and Gatley (1983) are more than 10″ offset from our improved radio positions, suggesting that their infrared objects may not be associated with the OH masers.

Accurate positions for the galactic-center sample were determined with the VLA on 1981 May 7. At this time, by using a bandpass of 390 kHz and 64 autocorrelation channels of 6.1 kHz each, 13 telescopes could be employed, covering a range in baselines from 0.2 to 10.5 km. The synthesized beam was 7″ × 4″. Instrumental phase calibration was effected using the standard calibration source 1748−253 and the low-elevation, secondary calibration source 1741+038. The names of the stars and their radio positions are listed in Table 2 in columns (1), (2), and (3). The data on 1741−038 show that the positional uncertainty due to systematic phase errors is less than 0″.1.

Single-dish OH fluxes of the tangential stars were measured with the Dwingeloo 25 m radio telescope in 1980, within 20–60 days of the Wyoming infrared observations (see § II*c*). Since this time difference is much less than 10% of the typical periods for these stars (Herman 1983), the infrared and radio fluxes can be considered coeval. Fluxes for the galactic-center sample were measured with the 85 foot (26 m) telescope at Hat Creek between 1981 August 27 and September 1, one month after the infrared observations on the IRTF (see § II*c*). No single-dish OH observations were made at the time of the UKIRT infrared observing run in 1982.

The high spectral resolution of the single-dish measurements (0.46 km s^{-1}) provided very accurate velocities and peak fluxes. Tables 1 and 2 contain the measured radio parameters of the two velocity components of the OH emission profiles for the tangential and the galactic-center samples respectively; radial velocities with respect to the local standard of rest, of the low- and high-velocity (LV, HV) peaks of the OH line profile are presented in columns (6) and (7) of Table 1 and columns (4) and (5) of Table 2; the corresponding peak flux densities, S_{LV} and S_{HV}, are shown in columns (8) and (9) of Table 1 and columns (6) and (7) of Table 2. The 1 σ uncertainty in the OH flux density measurement of the tangential sample is listed in the last column of Table 1.

c) Infrared Observations

Infrared observations of the tangential sources were made at the Cassegrain focus of the Wyoming Infrared Telescope (WIRO) in August, 1979 and 1980, using a helium-cooled bolometer (Bentley 1980). The aperture and chopper throw were 7″.5 and 20″ respectively. Infrared observations of the galactic-center sample were made at the IRTF and UKIRT on Mauna Kea, Hawaii, in 1981 July and 1982 June respectively, using the standard helium-cooled bolometers and also the liquid nitrogen–cooled InSb photometer at the UKIRT. A 6″ aperture was employed at the IRTF and one of 7″.5 at the UKIRT; chopper throws were 15″ EW at IRTF and 30″ in declination at UKIRT. Time did not allow us to observe all the stars in Table 2.

In general, measurements of the infrared counterparts of the OH/IR stars were made by integrating on the VLA positions using a broad-band filter centered at 10 μm, where the energy distributions usually peak and where confusion by foreground K and M giants is negligible. However, for a few galactic-center sources, searches at UKIRT were carried out at 8.7 or 20 μm when the earlier IRTF observations had shown that either the 10 μm absorption feature was sufficiently strong to preclude a 10 μm detection or that the energy distribution peaked longward of 12.5 μm. Infrared positions determined for the stronger sources from a five-point grid centered on the VLA positions agreed well with the radio positions. Long integrations adjacent

TABLE 3

FILTER CHARACTERISTICS

WIRO		Zeroth Mag	IRTF		UKIRT		Zeroth Mag[a]
λ (μm)	$\Delta\lambda$ (μm)	F_ν (Jy)	λ (μm)	$\Delta\lambda$ (μm)	λ (μm)	$\Delta\lambda$ (μm)	F_ν (Jy)
2.3	0.7	598	...	...	...	...	...
3.6	1.2	277	3.8	0.67	3.8	0.65	238
4.9	0.7	158	4.8	0.57	4.8	0.60	153
8.7	1.0	54	8.7	1.19	8.7	1.2	50
...	...	...	9.8	1.0	9.7	1.0	40
10.0	5.8	41	10.3	1.03	10.3	1.25	34
11.4	2.0	32	11.6	1.26	11.6	1.17	28
12.6	0.8	26	12.5	1.17	12.5	1.25	24
19.5	5.8	12	2.0	9.0	20.9	6.0	10

[a] Applies to both UKIRT and IRTF.

to the radio positions of a few objects yielded no detections. We are therefore confident that the infrared sources can be identified unambiguously with the OH stars.

Following the detections of the IR counterparts, photometric measurements between 3 and 20 μm were made. Appropriate filter characteristics are presented in Table 3. After taking account of the relevant air-mass corrections, magnitudes at each wavelength were determined from comparison with standard stars. Conversion from magnitudes to flux densities was accomplished using the values shown in Table 3 (cf. Gehrz, Hackwell, and Jones 1974; Beckwith *et al.* 1976). The measured infrared flux densities and 3 σ upper limits for the tangential sample are given in Tables 4 and 5, while those for the galactic-center sample are in Table 6. In both tables, the year in which the observations were made is indicated in column (2). Corresponding infrared energy distributions are shown in Figures 1 and 2 respectively. For wavelengths between 3.8 and 12.5 μm the uncertainties in the fluxes are of order $\pm 10\%$, and at 20 μm about 15%. Typical error bars for the shorter wavelengths are plotted at the 8.7 μm data point in each source energy distribution. Error bars for the 20 μm flux are also indicated.

TABLE 5

UPPER LIMITS FOR TANGENTIAL STARS (1980 Observations)

Name	10 μm Flux Density (Jy)
OH 17.2.....	<2.9
OH 18.5.....	<2.5
OH 25.1.....	<2.5
OH 27.0.....	<3.2
OH 27.5.....	<4.5
OH 29.4.....	<4.0
OH 36.4.....	<2.6
OH 37.1.....	<3.1

III. RESULTS AND ANALYSIS

Long-term monitoring observations at 18 cm (Harvey *et al.* 1974; Jewell, Webber, and Snyder 1980; Herman 1983) show that L_{OH} and L_* change simultaneously, strongly suggesting that the OH maser is radiatively pumped. But from the observed correlation between L_{OH} and the shell size, and from the very broad OH luminosity distribution (cf. BHMW), BH have argued that L_{OH} is a steep function of the stellar mass-loss rate and more or less independent of L_*. This is also suggested by the observed correlation between L_{OH} and near-infrared colors (e.g., Jones, Hyland, and Gatley 1983; Engels 1982; Herman 1983). This raises the question of the relation between $\dot{M}$ and L_{OH}, and the nature of the underlying star. As a result of (1) homogeneity, (2) simultaneous radio and infrared observations, and (3) information at $\lambda > 10$ μm, the present sample allows a quantitative analysis of the data involving L_{OH}, L_*, and $\dot{M}$ and a better understanding of the influence of $\dot{M}$ on the maser pump efficiency. The physical parameters of the stars and their circumstellar shells, determined from the radio and IR observations described above, are summarized in Tables 7 and 8. Their derivation and the influence of extinction are discussed in Appendices A and B respectively.

a) The OH *Maser Flux and Stellar Luminosity*

L_{OH} ranges from 1–10 Jy kpc^2 for nearby, optically identified OH emitting Miras to 10–1000 Jy kpc^2 for the distant, OH

TABLE 4

INFRARED FLUX DENSITIES OF TANGENTIAL OH/IR STARS (Jy)

		Wavelength (μm)							
Name	Date	2.3	3.6	4.9	8.7	10.0	11.4	12.6	19.5
OH 10.8+1.5.....	1980	...	0.1	...	11.7	3.8	3.9	12.9	29.1
OH 18.2+0.5.....	1980	...	0.7	...	10.7	8.1	6.1	15.2	<12.8[a]
OH 20.7+0.1.....	1979	...	<0.2[a]	0.8	2.3	2.5	0.9	5.8	7.9
OH 21.5+0.5.....	1979	<0.1[a]	2.1	20.6	35.0	29.2	16.7	63.4	68.5
OH 24.7−0.1.....	1979	0.9	11.6	27.7	30.5	24.5	22.0	33.6	28.3
OH 27.2+0.2.....	1979	0.2	2.2	5.0	8.3	7.8	8.8	10.7	9.2
OH 27.8−1.5.....	1980	3.2	14.7	...	38.8	37.7	37.2	38.6	31.6
OH 28.5−0.0.....	1980	...	0.3	...	6.5	7.4	...	<6.8[a]	...
OH 30.1−0.7.....	1979	<0.1[a]	1.4	16.9	68.6	53.6	28.7	100.5	129.4
OH 31.0−0.2.....	1980	...	<0.2[a]	...	19.8	14.1	<14.7[a]	24.8	19.4
OH 32.0−0.5.....	1979	<0.1[a]	0.1	2.8	5.9	6.4	3.9	13.6	15.6
OH 32.1+0.9.....	1980	0.1	1.5	...	12.0	<7.0[a]	...	11.4	...
OH 34.9+0.8.....	1980	<0.1[a]	1.8	...	10.1	6.6	...	10.3	...
OH 37.7−1.4.....	1980	<0.1[a]	1.1	3.7	7.1	8.3	...	<5.4[a]	...
OH 39.9−0.0.....	1979	<0.1[a]	1.1	4.9	11.6	9.2	6.8	15.4	15.6

[a] Upper limits are 3 σ.

TABLE 6

INFRARED FLUX DENSITIES OF OH/IR SOURCES IN THE GALACTIC CENTER
(Jy)

NAME	DATE	WAVELENGTH (μm)							
		3.8	4.8	8.7	9.7	10.5	11.5	12.5	19.8
OH 359.1+1.1	1982	<0.2[a]	0.08	0.31	0.34	...	...	1.04	3.13
	1981	...	0.11	0.61	0.73	0.79	1.61	2.33	10.67
OH 359.4+0.1	1982	...	...	<0.2[a]	...	...	...	0.45	<1.6[a]
	1981	...	0.23	0.52	0.27	...	0.56	1.87	2.21
OH 0.2+0.0	1982	0.95	1.24	1.73	0.38	0.31	1.73	1.85	2.60
	1981	...	0.58	0.47	0.09	<0.2[a]	0.60	0.5	0.50
OH 0.3−0.2	1981	...	...	...	...	...	...	0.45	1.2
OH 0.5−0.2	1982	...	0.33	0.70	<0.4[a]	...	073	1.10	1.27
	1981	...	0.51	1.04	0.24	0.29	1.18	3.13	3.2
OH 1.08+0.4	1981	...	<0.3[a]	...	...	<0.2[a]	...	0.23	4.2
OH 2.6−0.4	1982	78.09	80.30	197.23	159.24	167.29	191.94	112.78	167.49
OH 4.0−0.9	1982	...	<0.2[a]	0.63	0.84	...	...	<2.1[a]	5.25
OH 4.6−0.4	1982	3.60	4.93	8.53	1.36	1.63	7.78	9.91	8.95
	1981	...	6.44	8.06	2.11	2.33	9.23	17.42	23.3
OH 9.6+0.5	1982	7.88	6.44	18.32	14.93	15.40	11.83	15.43	15.85
	1981	...	5.93	16.72	19.23	17.88	19.52	19.08	17.0

[a] Upper limits are 3 σ.

luminous, but optically obscured, OH/IR stars studied in this paper. The OH luminosity of these objects increases steeply with decreasing L_{OH}, and it has been suggested that Miras may represent the low-luminosity tail (BHMW). Values of L_* for Miras and OH/IR stars are not significantly different, leading to the hypothesis that L_{OH} is independent of L_* (BH). Indeed, the present data support this contention; in Figure 3, where the tangential sources are plotted as filled circles and the galactic-center sample is represented by crosses, there is no evidence of a strong correlation between L_{OH} and L_*.

L_{OH} for the galactic-center sample is a factor of 2 to 3 smaller than that for the tangential sample, reflecting the higher sensitivity of the OH observations near the galactic center. The mean bolometric luminosity for the detected stars in the tangential sample is $3.4 \times 10^4\ L_\odot$, whereas it is $2 \times 10^3\ L_\odot$ for the stars in the vicinity of the galactic center ($l < 1°$). It is not clear whether this discrepancy is real. It could result from differences in the sensitivity and completeness of each sample or from the variations between the space density of OH/IR stars near the galactic center and in the disk near tangential point. Although OH/IR stars in the galactic center have much lower bolometric luminosities than those at the tangential point, a larger interstellar extinction toward the galactic center could to some extent explain the disparity. It is, however, unlikely that it can account for a discrepancy of more than a factor of 2, indicating that the OH/IR stars in the bulge are intrinsically at least 5 times less luminous than those in the disk.

Figure 4 demonstrates that there is no correlation between L_{OH} and v_e, the shell expansion velocity. Given the absence of a correlation in Figure 3, this is scarcely surprising because, for OH/IR stars, v_e is statistically related to the main-sequence mass (BHMW). Since the main-sequence mass is related to the AGB mass (cf. Iben 1981), which in turn determines the bolometric luminosity (Paczyński 1970), v_e and L_* should in fact be correlated. The statistical data of Jones, Hyland, and Gatley (1983) appear to support such a correlation and, although the scatter in Figure 5 is large, there is a weak trend for the most luminous stars to have higher values of v_e.

b) The OH Maser Flux and the Circumstellar Dust Density

The long-term variability and bolometric luminosity of these OH/IR stars suggest that their stellar parameters are similar to those of the OH emitting Miras with effective temperatures between 2500 and 3500 K and maxima in the energy distributions between 1 and 2 μm (cf. Merrill 1977). It is commonly thought that the OH maser is pumped by 35 μm photons (Elitzur, Goldreich, and Scoville 1976), but in the case of the OH luminous OH/IR stars, the stellar photospheric flux at 35 μm is clearly insufficient to provide enough maser pump photons. This implies that the maser luminosity depends on the efficiency with which the stellar light is converted to 35 μm emission in the circumstellar shells, i.e., on the dust-column density. If the pumping is due to 35 μm photons and the maser is saturated, then stars with the same OH luminosity but different values of L_* produce similar 35 μm fluxes, and the energy distributions must be redder and cooler for lower values of L_*. Thus the ratio L_{OH}/L_* should be positively correlated with the fraction of the total energy that is emitted at 35 μm.

In Figure 6 L_{OH}/L_* is plotted against the fraction of the total energy emitted at 20 μm, $\lambda F_{20}/F_{IR}$. Since in most cases the maximum in the energy distribution of these objects lies shortward of 35 μm, $\lambda F_{20}/F_{IR}$ is a reasonable measure of the relative amount of energy emitted at 35 μm. Both L_{OH}/L_* and $\lambda F_{20}/F_{IR}$ are distance-independent. The OH luminosity increases steeply with the fraction of the total emission that emerges at 20 μm, that is, when the energy distribution becomes redder. It is clear from this figure that for most stars there is a remarkably tight correlation between the two quantities, which is intrinsic and cannot be due to variable interstellar extinction. Three objects, OH 359.1, OH 4.6, and OH 10.9, which lie significantly below the observed correlation, have anomalously low OH luminosities. OH 0.2 lies well above the trend and appears to emit more OH photons than 35 μm pump photons, in violation of the simple 35 μm pump model (Elitzur, Goldreich, and Scoville 1976). This discrepancy is discussed in § IV.

A linear regression fit, excluding the four anomalous sources

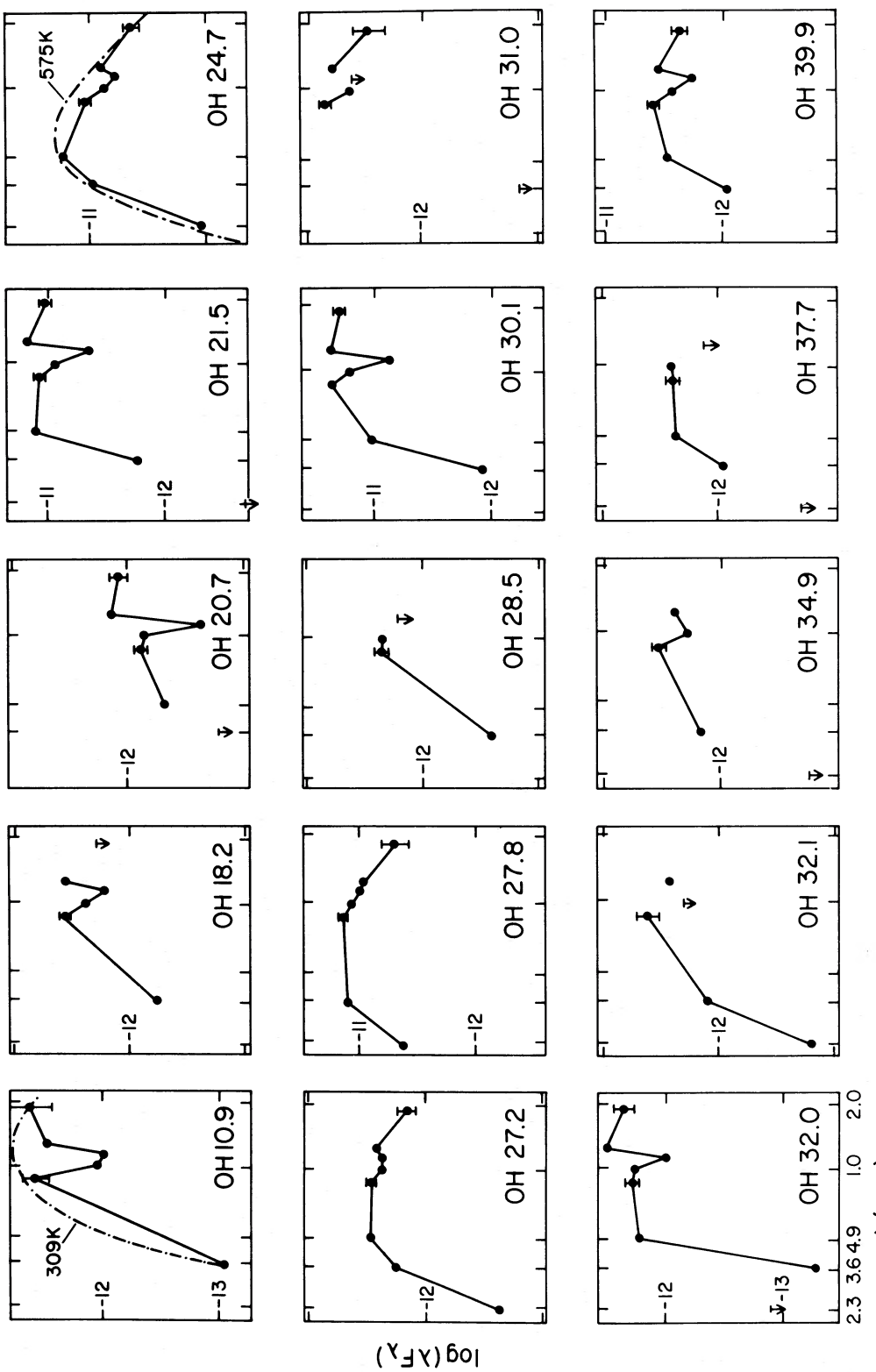

FIG. 1.—Infrared energy distributions of the tangential OH/IR stars measured at WIRO. The flux scale is in units of W m^{-2}. Upper limits are indicated by an arrow, uncertainties by a bar at the 8.7 and 20 μm points. Examples of a blackbody fit are given for OH 10.9 and OH 24.7.

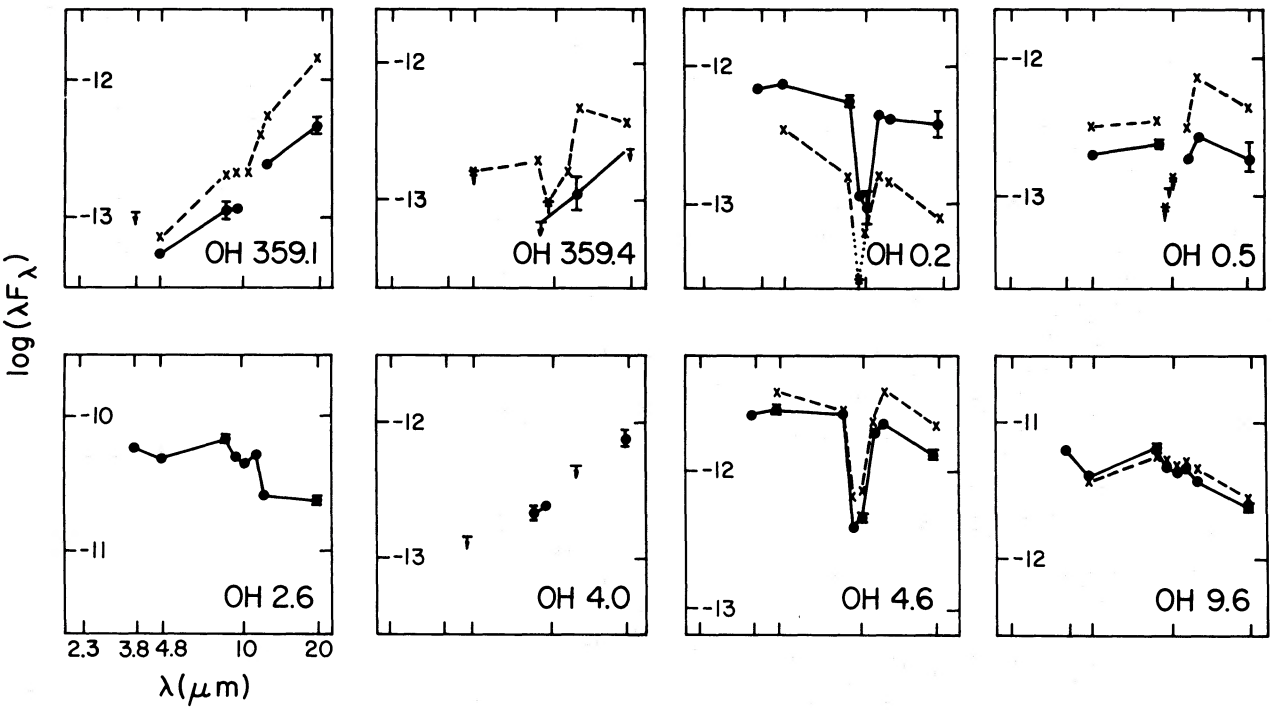

FIG. 2.—Infrared energy distributions of the galactic center sample measured with IRTF in 1981 (*continuous*) and with UKIRT in 1982 (*dashed*)

and the upper limit for OH 18.2, yields

$$\log\left(\frac{L_{\rm OH}}{L_*}\right) = 2.4(\pm 0.1)\log\left(\frac{\lambda F_{20}}{F_{\rm IR}}\right) - 0.5(\pm 0.03)\,. \quad (1)$$

The harmonic mean OH flux, $S_{\rm OH}$, is then given by

$$S_{\rm OH} = 0.9 F_{\rm IR}\left(\frac{\lambda F_{20}}{F_{\rm IR}}\right)^{2.4} \text{Jy}\,, \quad (2)$$

with $F_{\rm IR}$ and λF_{20} in units of 10^{-13} W m^{-2}. The dependence of $S_{\rm OH}$ on $F_{\rm IR}$ and $\lambda F_{20}/F_{\rm IR}$ is consistent with the observations; the OH maser output follows closely the time variations in L_*, as would be expected from $S_{\rm OH} \propto F_{\rm IR}$. In addition, the steep dependence of $S_{\rm OH}$ on $\lambda F_{20}/F_{\rm IR}$ implies that no direct correlation is expected between L_* and $L_{\rm OH}$ (cf. Fig. 3); the relative amount of long-wavelength flux, which is a function of the dust-column density and hence the mass-loss rate, rather than

TABLE 7

RADIO AND INFRARED PROPERTIES OF TANGENTIAL OH/IR STARS

Name	Distance[a] (kpc)	$L_{\rm OH}$[a] (Jy kpc^2)	v_e (km s^{-1})	$F_{\rm IR}$ (10^{-13} W m^{-2})	L_*[a] ($10^4 L_\odot$)	T_c (K)	$\tau_{\rm sil}$
OH 10.9+1.5.....	8.5–11.8	120–230	16.25	63 ± 7	1.34–2.58	310	1.3
OH 17.2−1.1.....	9.6	240	12.50	...	...	...	...
OH 18.2+0.5.....	9.5	150	12.15	50 ± 6	1.33	410	0.9
OH 18.5+1.4.....	9.5	620	10.65	...	...	...	...
OH 20.7+0.1.....	9.4	720	18.30	18 ± 2	0.47	350	1.8
OH 21.5+0.5.....	8.6–10.1	2170–2990	18.20	260 ± 30	5.68–7.83	410	1.2
OH 24.7−0.1.....	9.1	220	16.50	265 ± 30	6.48	580	0.4
OH 25.1−0.3.....	9.1	590	12.40	...	...	...	...
OH 27.0−0.4.....	7.4–10.4	300–590	14.60	...	...	...	...
OH 27.2+0.2.....	6.7–11.1	90–260	19.40	60 ± 7	0.80–2.18	520	0.2
OH 27.5−0.9.....	8.9	520	13.50	...	...	...	...
OH 27.8−1.5.....	6.1–11.6	90–340	15.20	340 ± 40	3.73–13.5	620	<0.1
OH 28.5−0.0.....	8.8	900	13.35	49 ± 6	1.12	>380	...
OH 29.4−0.8.....	8.7	590	11.85	...	...	...	...
OH 30.1−0.7.....	7.3–10.0	3110–5840	20.30	380 ± 45	5.98–11.2	360	1.2
OH 31.0−0.2.....	8.6	430	14.35	96 ± 10	2.10	<340	>0.4
OH 32.0−0.5.....	5.4–11.6	190–880	20.50	45 ± 5	0.39–1.79	410	1.0
OH 32.1+0.9.....	8.5	220	12.30	75 ± 9	1.60	500	...
OH 34.9+0.8.....	4.8–11.6	60–370	14.45	56 ± 7	0.38–2.22	490	0.5
OH 36.4+0.3.....	8.1	240	18.85	...	...	...	...
OH 37.1−0.8.....	8.0	240	13.25	...	...	...	...
OH 37.7−1.4.....	7.9	70	10.00	56 ± 7	1.03	>490	...
OH 39.9−0.0.....	7.7	280	14.65	70 ± 8	1.23	430	0.8

[a] In case of a distance ambiguity, values for both the near- and the far-kinematic distance are given.

TABLE 8

RADIO AND INFRARED PROPERTIES OF THE GALACTIC CENTER OH/IR STARS

Name	Distance (kpc)	L_{OH} (Jy kpc^2)	v_e (km s^{-1})	F_{IR} (10^{-13} W m^{-2})	L_* (10^4 $L_\odot$)	T_c (K)	τ_{sil}	Year
OH 359.1	10	...	9.25	5.4	0.16	340	...	1982
		250	...	12.6	0.37	300	0.2	1981
OH 359.4	10	...	12.25	<1.4	<0.04	<230	...	1982
		130	...	<4.5	<0.13	<370	>1.0	1981
OH 0.2	10	...	14.5	11.9	0.34	590	1.6	1982
		90	...	3.4	0.1	450	2.1	1981
OH 0.3	10	210	14.5	>1.2	>0.04	...	...	1981
OH 0.5	10	...	11.75	3.8	0.11	460	>0.8	1982
		120	...	8.1	0.24	400	>1.7	1981
OH 1.08	10	<60	17.0	<4.8	<0.14	...	...	1981
OH 2.6	5	340[a]	22.75	936	6.8	600	0.2	1982
OH 4.0	10	110[a]	14.5	<6.6	<0.19	370	...	1982
OH 4.6	10	...	23.0	56	1.6	530	1.8	1982
		210	...	89	2.6	500	1.6	1981
OH 9.6	10	...	23.5	90	2.6	500	0.2	1982
		260		98	2.9	460	<0.1	1981

[a] 1981 measurement.

the integrated flux (stellar luminosity), is the dominant parameter governing the maser flux. That is to say, the OH luminosity depends mainly on the effective temperature of the circumstellar dust (see § IIIc), with an overall scaling factor due to the bolometric luminosity. Since the precise relation between the relative amount of 20 μm flux and $\dot{M}$ is not known, a direct comparison between L_{OH}/L_* and $\dot{M}$ is not possible.

c) Silicate Absorption

The silicate absorption feature at 9.7 μm is formed in the cool outer regions of the circumstellar shell. Its apparent depth, τ_{sil}, is a measure of the dust-column density and is also expected to be inversely proportional to T_c (Kwan and Scoville 1976). Since τ_{sil} appears to be correlated with L_{OH}/L_* (Herman 1983), it should increase with $\lambda F_{20}/F_{IR}$; Figure 7*a* shows that this is indeed the case, although OH 0.2 and OH 4.6 have unexpectedly high values of τ_{sil}. Both objects are also anomalous in Figure 5. OH 359.1 is extremely red but has a low value of τ_{sil}, similar to OH 17.7−2.0 (Olnon *et al.* 1984), suggesting that in the coolest objects, which presumably experience the largest mass-loss rate, the formation of the silicate feature is severely inhibited by an as yet unspecified mecha-

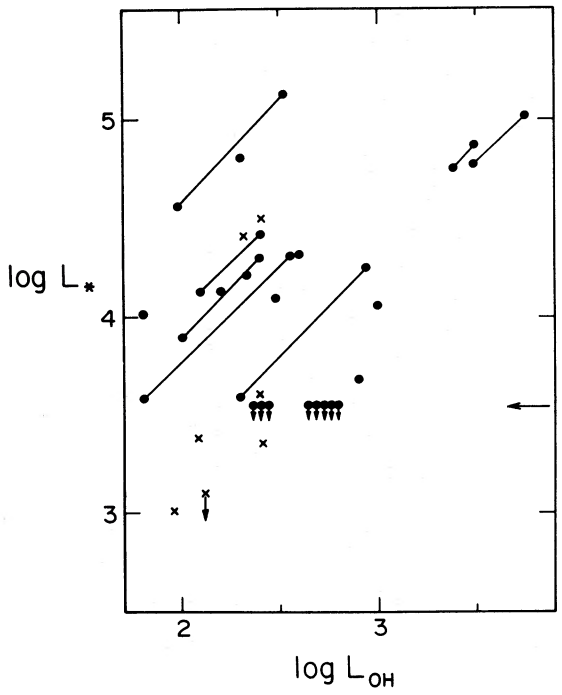

FIG. 3

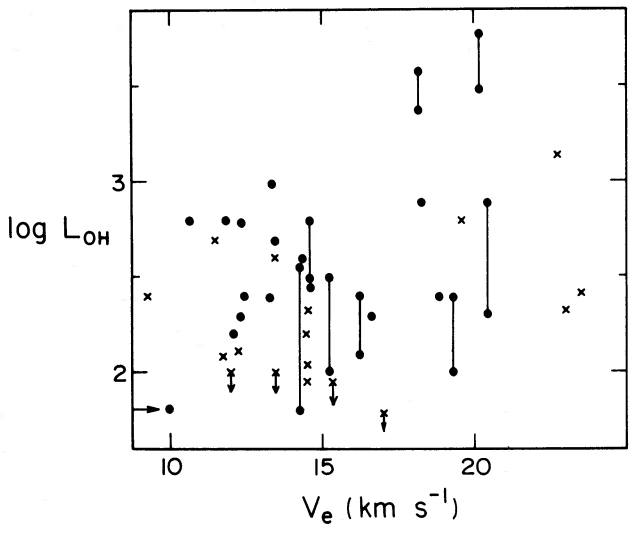

FIG. 4

FIG. 3.—The stellar bolometric luminosity L_* in $L_\odot$ as a function of the maser luminosity L_{OH} in Jy kpc^2. In this and the following figures the tangential sample is indicated by filled circles, the galactic-center sample by crosses. Values corresponding to the near- and far-kinematic distances for the tangential sample are connected by a line. The arrow indicates the sensitivity limit for the WIRO measurements (see text).

FIG. 4.—The maser luminosity as a function of v_e, the outflow velocity of the circumstellar shell

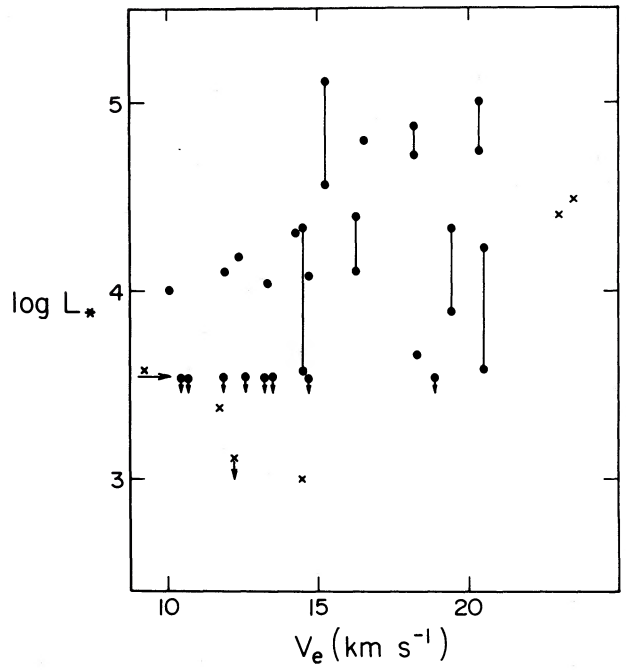

FIG. 5

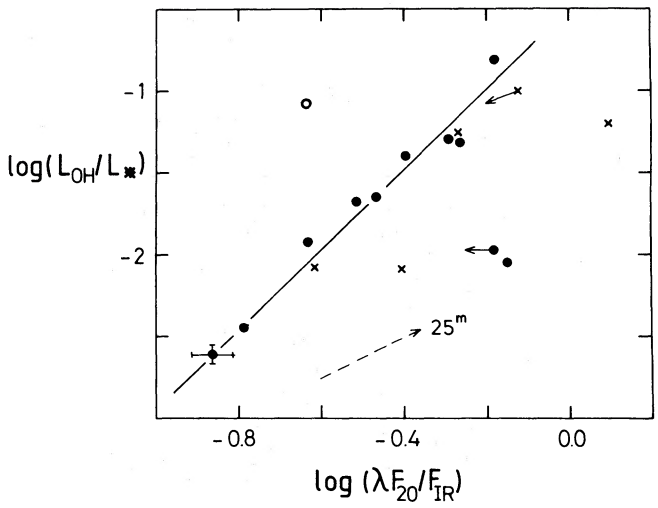

FIG. 6

FIG. 5.—Bolometric luminosity as a function of outflow velocity

FIG. 6.—The ratio of maser to bolometric luminosity as a function of the fraction of total infrared energy emitted at 20 μm. The open circle represents OH 0.2 (see text). L_{OH} and L_* are in the same units as in Fig. 3. Infrared energies are in W m^{-2}. The dashed arrow indicates the effect of 25 mag of visual extinction (see Appendix B). The solid line is a least-squares fit through the tangential sample, excluding the anomalous sources (see eq. 1). Typical error bars are indicated.

nism. A linear fit through all data points except the limits and the two anomalous stars gives the following relation:

$$\tau_{sil} = 2.1(\pm 0.2) \log\left(\frac{\lambda F_{20}}{F_{IR}}\right) + 1.8(\pm 0.2)\,, \qquad (3)$$

with a correlation coefficient of 92%. Figure 7*b* confirms that the silicate optical depth is proportional to T_c^{-1}.

An insterstellar component in the silicate absorption feature has not yet been completely ruled out. In a small sample of OH/IR stars, Evans and Beckwith (1977) found no correlation between τ_{sil} and distance, arguing for a circumstellar origin. If the silicate feature were due solely to interstellar extinction, no correlation with $\lambda F_{20}/F_{IR}$ would be seen in Figure 7*a* and, indeed, τ_{sil} would be expected to depend on galactic latitude. Since this is not the case, the possibility of the silicate feature arising in the interstellar medium can be ruled out.

IV. DISCUSSION

Our simultaneous radio and infrared observations of two samples of distant OH/IR stars at the tangential point and the

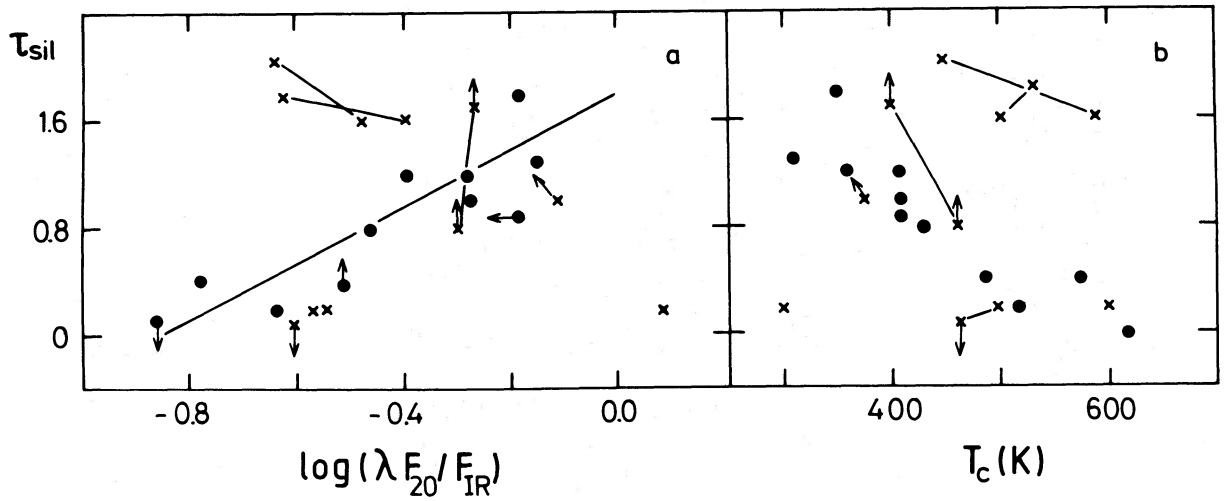

FIG. 7.—The apparent silicate optical depth as a function of (*a*) the fraction of infrared energy emitted at 20 μm and (*b*) the color temperature between 4.8 and 12.5 μm. The solid line in (*a*) is a least-squares fit to the tangential sample (see eq. 3).

galactic center demonstrate that the OH luminosities of these objects are dependent on the fraction of the total infrared energy which is emitted near 35 μm, which in turn is a measure of the mass-loss rate. Sources with the same stellar parameters, such as bolometric luminosity and mass, may have widely different circumstellar properties. This is reflected in large variations in L_{OH} among stars with similar values of v_e and L_*. For a given bolometric luminosity, stars with higher OH luminosity have redder infrared energy distributions and deeper silicate absorption features, indicative of cooler circumstellar shells and higher mass-loss rates.

a) *Maser Pump Efficiency*

Equations (1) and (2) show that for a given star L_{OH} is a function of the relative amount of long-wavelength photons produced in the circumstellar shell. In the 35 μm pumping scheme the observed maser pump efficiency ϵ is given by

$$\epsilon = \frac{S_{OH}}{S_{35}} A_{35} \frac{\Omega_{OH} \delta v_{OH}}{\Omega_{35} \delta v_{IR}}$$

(cf. Evans and Beckwith 1977), where S, Ω, and δv are the flux densities, the solid angles into which the flux is emitted, and the bandwidths in km s^{-1} for OH emission and 35 μm absorption respectively, and A_{35} is the interstellar attentuation. In the simplest case, the last three factors are 1 and the predicted efficiency for a saturated maser, given by the flux density ratio, is 0.25 (Elitzur, Goldreich, and Scoville 1976).

For the present stars S_{35} was estimated from a linear extrapolation between 12 and 20 μm. The derived ratio S_{OH}/S_{35} is plotted in Figure 8 against $\lambda F_{20}/F_{IR}$. Given the uncertainties, the flux-density ratio, reflecting the efficiency, is generally close to the expected value of 0.25. Nevertheless, there is some indication of a trend for the flux-density ratio to increase from 0.15 to 0.6 with increasing circumstellar reddening, suggesting a corresponding increase in the observed pump efficiency. This can be reconciled with the expected value $\epsilon = 0.25$, if the bandwidth ratio $\delta v_{OH}/\delta v_{35}$ decreases with increasing thickness of the circumstellar shell. When the shell becomes thicker, the radius at which the majority of 35 μm pump photons are produced grows, and δv_{35} increases due to the changing geometry between the maser-emitting region and the 35 μm pump region (cf. Evans and Beckwith 1977).

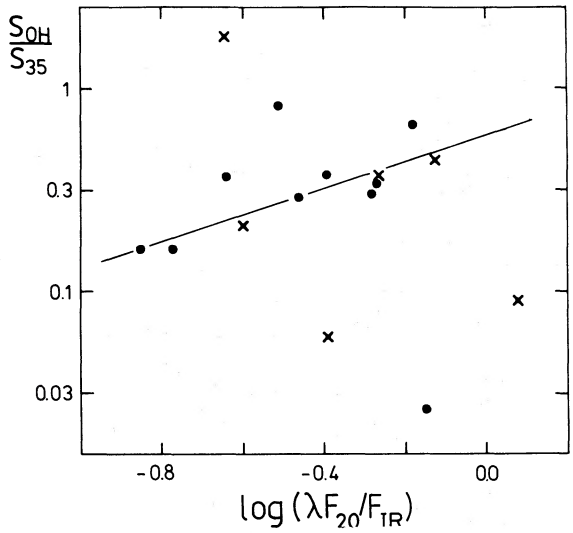

FIG. 8.—The ratio of OH to 35 μm flux as a function of the fraction of the infrared energy emitted at 20 μm.

b) *Variations in the Silicate Absorption Depth*

Our results also indicate that, for a given star, as L_* declines, an increase in the silicate absorption feature τ_{sil}, should result. While the luminosity of the OH maser changes in phase with the bolometric luminosity of the central star, the amplitude of the variation is about a factor of 2 smaller (e.g., Herman 1983), with

$$\frac{F_{max}}{F_{min}} = 2 \frac{S_{max}}{S_{min}}, \tag{4}$$

where $S_{max, min}$ and $F_{max, min}$ are respectively the OH and bolometric fluxes at the maximum and minimum of the light curve. Thus, the relative amount of 35 μm flux, which reflects the temperature of the outer dust shell, should change as a function of phase in the light curve. Since the depth of the silicate feature indicates a temperature gradient between the regions where the 10 μm continuum and silicate features arise (Kwan and Scoville 1976), τ_{sil} should also vary over the light curve. From equations (2) and (4) it can be shown that

$$\left(\frac{\lambda F_{20}}{F_{IR}}\right)_{max} = 0.75 \left(\frac{\lambda F_{20}}{F_{IR}}\right)_{min}. \tag{5}$$

Thus, combining equations (5) and (3), the change in the silicate optical depth between minimum and maximum of the light curve is given by

$$\Delta\tau = \tau_{min} - \tau_{max} \approx 0.26,$$

where $\tau_{min, max}$ are the silicate optical depths at minimum and maximum light. Because of the large width of the 10 μm filter used at WIRO, the precise value of $\Delta\tau$ is uncertain, but effectively the relation implies that the silicate optical depth is smaller at maximum light than at minimum and should increase with decreasing L_*. This is in good qualitative agreement with our observations of those stars in the galactic-center sample for which infrared fluxes were measured at two epochs (cf. Fig. 2 and Table 6) and with the measurements of the bright OH/IR star OH 26.5+0.6 (Forrest *et al.* 1978).

c) *Circumstellar Shell Size and* OH *Luminosity*

The correlation found between L_{OH} and the size of the circumstellar shell by BH can now be understood. As the mass-loss rate increases, the circumstellar shell density rises so that the OH maser can operate at larger radii from the star; the minimum density required for a saturated maser, $n_H = 10^4$ (cf. Elitzur, Goldreich, and Scoville 1976) is found over a greater surface area. Since the stimulated-emission rate for a saturated maser is determined by the number of pump photons, L_{OH} will not be enhanced merely by enlarging the maser volume. Nevertheless, with rising density the circumstellar dust becomes cooler and more stellar emission is converted to 35 μm flux. Thus, with increasing mass-loss rate, the effects of a higher number of pump photons and of available OH molecules combine to produce enhanced maser emission and keep the maser saturated.

V. CONCLUSIONS

In this paper we have presented simultaneous OH and infrared measurements of a homogeneous sample of OH/IR stars at

the tangential point and near the galactic center; their distances are therefore well known. Very accurate radio positions, derived from VLA observations, and identifications of the infrared counterparts at wavelengths longward of 8 μm reduce the possibility of confusion. We find that the characteristics of the objects in each sample are very similar in most respects. Although there is some tendency for the luminosities of the galactic-center stars to be lower than those at the tangential point, the paucity of objects makes it difficult to ascertain whether this is significant. Future studies, perhaps based on the results of the IRAS survey, should make it possible to verify whether a population of low-luminosity masers indeed exists in the galactic bulge.

As a result of the homogeneity of the samples, the reliability of the infrared identifications, and the simultaneous radio and infrared measurements, it has been possible to establish a number of relations between various stellar and circumstellar properties. In particular, it has been shown quantitatively that the OH luminosity is dominated by the fraction of the infrared energy emitted longward of 20 μm and thus by the stellar mass-loss rate. However, L_{OH} is to some extent dependent on the bolometric luminosity so that, as observed, time variations in L_* are reflected in L_{OH}. It has also been demonstrated that the apparent optical depth of the silicate feature τ_{sil} is determined by the stellar mass-loss rate, confirming that this feature arises in the circumstellar shell. Moreover, using the dependence of both L_{OH} and τ_{sil} on the stellar mass-loss rate, and the fact that the amplitude of variability of the OH maser emission is half that of the stellar emission, the observed variations in τ_{sil} over the light curve of a given object can be explained in a qualitative manner.

Our new data have permitted an investigation of the maser pump efficiency. Within the uncertainties, this is found to be consistent with the canonical value of 0.25. However, some tendency for the inferred efficiency to increase with increasing circumstellar reddening is discernible in the data.

The results discussed above were derived from a sample of stars covering a wide range of masses and luminosities. Although these objects represent the high-luminosity tail of the OH luminosity distribution, it seems justifiable to extend our conclusions to the majority of OH/IR stars. In particular, it is clear that sources whose stellar properties are the same can have a variety of circumstellar attributes. In effect, for a given L_* a large range of values of L_{OH}, which reflect differing mass-loss rates, is possible. Thus these stars can be interpreted as representing an evolutionary sequence of increasing mass-loss rate.

The measurements described here were made at six observatories in the course of seven observing runs. As a result, thanks are due to many people for their contributions to the success of the project. We are grateful to the staff of WIRO for providing observing time and for their willing and competent assistance. At the IRTF and UKIRT, R. Isaacman helped with the observations. In particular we thank I. Gatley for his support at the UKIRT. J. Herman kindly made observations for us at Dwingeloo. At Hat Creek, M. Stevens most ably carried out the measurements, while the VLA results were made possible with help from A. Rots, J. Dreher, and R. Perley. Especially, we would like to thank J. Turner and S. Kulkarni, who carried out a major part of the VLA spectral-line data reduction. We are grateful to N. Scoville for a critical reading of the manuscript and to the referee, T. J. Jones, for helpful comments. This work was begun while one of us (B. B.) was at the Radio Astronomy Laboratory at U.C. Berkeley and was supported by NSF grant AST78-21037; J. Welch is thanked for his help and encouragement. A. I. S. is supported by NSF grant AST 82-10828 to the Owens Valley Radio Observatory.

APPENDIX A

DERIVED PHYSICAL PARAMETERS FOR OH/IR STARS

The *distance* to the OH/IR stars studied here, D, is based on a galactic distance scale, center-to-Sun, of $R_\odot = 10$ kpc. For the tangential sample it is derived kinematically from the stellar radial velocity $v = (\mathrm{HV} + \mathrm{LV})/2$ (km s^{-1}) (where HV and LV are the velocities with respect to the local standard of rest of the high- and low-velocity components of the OH profile), using the galactic rotation curve of Burton and Gordon (1978). For stars with radial velocities larger than the maximum velocity allowed by circular rotation v_{max}, D is presumed equal to the distance to the tangential point. Stars with $v < v_{max}$ probably lie between the listed near- and far-kinematic distances. For the galactic-center sample, stars within a degree of the center have high radial velocities ($|v| > 100$ km s^{-1}) and are assumed to be part of the bulge population at a distance of 10 kpc (Habing *et al.* 1983). At $l > 1°$, where the density of the bulge drops off significantly, distances are more uncertain. Objects with small radial velocities ($|v| \leq 10$ km s^{-1}) are probably foreground stars and are assumed to be at the location of the molecular ring at 5 kpc distance, where the density distribution of the OH/IR stars peaks (cf. BHMW). The remainder of the sample, with high negative or positive radial velocities, is assumed to be at a distance of $10 \pm 10l$ kpc, where l is the source galactic longitude in radians.

The *expansion velocity* of the circumstellar shell is $v_e = (\mathrm{HV} - \mathrm{LV})/2$ (km s^{-1}).

The *OH luminosity* L_{OH} at 1612 MHz is $L_{OH} = D^2(S_{LV}\,S_{HV})^{1/2}$ (Jy kpc^2), where D is in kpc (cf. BHMW). The 3 σ sensitivity limit of the Dwingeloo and Onsala survey, from which the tangential sample was drawn, is $\sim$0.6 Jy. At a mean distance of 8.9 kpc this corresponds to a minimum detectable OH luminosity of 50 Jy kpc^2 and to a completeness limit of 100 Jy kpc^2. For the galactic-center sample, similar values apply.

Regarding *stellar luminosity*, most energy distributions in Figures 1 and 2 rise between 3 and 8.7 μm and many appear to be broader than expected for a single-temperature Planck curve, indicating the presence of circumstellar dust at different temperatures. The stellar radiation, which peaks around 1–2 μm, is absorbed by the dense dust shell and reemitted at longer infrared wavelengths. The integrated infrared flux F_{IR} determined from the observed energy distribution, and including a correction factor of 25% to account for flux emitted beyond 25 μm (cf. Werner *et al.* 1980), is therefore a good measure of the bolometric luminosity of the star.

The stellar luminosity is then $L_* = 2.9D^2F_{IR}$ ($L_\odot$), where D is in kpc and F_{IR} is in 10^{-13} W m^{-2}. If the OH sources without infrared detections (Table 5) have energy distributions similar to those detected, their 10 μm upper limits correspond to $L_* \leq 3.5 \times 10^3\ L_\odot$ for a mean distance of 8.9 kpc.

The *color temperature* T_c for each source was determined by fitting a Planck curve to the observed infrared energy distribution between 4.8 and 12.5 μm.

As for *silicate absorption*, the optical depth of the silicate feature τ_{sil} seen at 9.7 μm in Figures 1 and 2 was derived from the ratio of the measured flux at the deepest point of the feature λF_{sil} to the continuum flux at the same wavelength λF_{cont}, interpolated from the 8.7 and the 12.6 μm flux measurements, so that $\tau_{sil} = -\ln(\lambda F_{sil}/\lambda F_{cont})$.

APPENDIX B

THE EFFECTS OF INTERSTELLAR EXTINCTION

Stellar parameters, such as the bolometric luminosity and the color temperature, which are derived from the infrared observations, will be influenced by interstellar extinction. This can range from 7 to 32 mag in the visual for these distant stars (de Jong 1983). Using the extinction law in the infrared from Becklin *et al.* (1978), we calculate that for an average visual extinction of 20–30 mag the observed luminosity of a 400 K blackbody will be underestimated by a factor of $\sim$1.6. Since both distance uncertainties and variations in the extinction with respect to the mean could cause uncertainties in the derived bolometric luminosities of a factor of 2–3 for individual objects, no corrections for interstellar extinction were made. However, the influence of 25 mag of extinction on a blackbody of 400 K is shown in Figure 3 by an arrow. None of the trends discussed in the body of the text appear to be significantly influenced by interstellar extinction.

REFERENCES

Baud, B., and Habing, H. J. 1983, *Astr. Ap.*, **127**, 73 (BH).
Baud, B., Habing, H. J., Matthews, H. E., and Winnberg, A. 1979*a*, *Astr. Ap. Suppl.*, **35**, 179.
———. 1979*b*, *Astr. Ap. Suppl.*, **36**, 193.
———. 1981, *Astr. Ap.*, **95**, 156 (BHMW).
Becklin, E. E., Matthews, K., Neugebauer, G., and Willner, S. P. 1978, *Ap. J.*, **220**, 831.
Beckwith, S., Evans II, N. J., Becklin, E. E., and Neugebauer, G. 1976, *Ap. J.*, **208**, 390.
Bentley, A. F. 1980, Ph.D. thesis, University of Wyoming.
Bowers, P. F. 1978, *Astr. Ap.*, **64**, 307.
Burton, W. B., and Gordon, M. A. 1978, *Astr. Ap.*, **63**, 7.
de Jong, T. 1983, *Ap. J.*, **274**, 252.
Elitzur, M., Goldreich, P., and Scoville, N. 1976, *Ap. J.*, **205**, 384.
Engels, D. 1982, Ph.D. thesis, Bonn.
Evans, N. J., and Beckwith, S. 1977, *Ap. J.*, **217**, 729.
Forrest, W. J., *et al.* 1978, *Ap. J.*, **219**, 114.
Gehrz, R. D., Hackwell, J. A., and Jones, T. J. 1974, *Ap. J.*, **191**, 675.
Habing, H. J., Olnon, F. M., Winnberg, A., Matthews, H. E., and Baud, B. 1983, *Astr. Ap.*, **128**, 230.
Harvey, P. M., Bechis, K. B., Wilson, W. J., and Ball, J. A. 1974, *Ap. J. Suppl.*, **27**, 331.
Herman, J. 1983, Ph.D. thesis, University of Leiden.
Iben, I. Jr. 1981, in *Effects of Mass Loss on Stellar Evolution*, ed. C. Chiosi and R. Stalio (Dordrecht: Reidel), p. 373.
Jewell, P. R., Webber, J. C., and Snyder, L. E. 1980, *Ap. J. (Letters)*, **242**, L29.
Johansson, L. E. B., Andersson, C., Goss, W. M., and Winnberg, A. 1977, *Astr. Ap. Suppl.*, **28**, 199.
Jones, T. J., Ashley, M., Hyland, A. R., and Ruelas-Mayorga, A. 1981, *M.N.R.A.S.*, **197**, 413.
Jones, T. J., Hyland, A. R., Caswell, J. L., and Gatley, I. 1982, *Ap. J.*, **253**, 208.
Jones, T. J., Hyland, A. R., and Gatley, I. 1983, *Ap. J.*, **273**, 660.
Jones, T. J., Hyland, A. R., Wood, P. R., and Gatley, I. 1983, *Ap. J.*, **273**, 669.
Kwan, J., and Scoville, N. Z. 1976, *Ap. J.*, **209**, 102.
Merrill, K. M. 1977, in *IAU Colloquium 42, The Interaction of Variable Stars with Their Environment*, ed. R. Kippenhahn, J. Rahe, and W. Strohmeier (Bamberg: Reimers-Sternwarte), p. 446.
Nguyen-Q-Rieu, Laury-Micoloulaut, C., Winnberg, A., and Schultz, G. V. 1979, *Astr. Ap.*, **75**, 352.
Olnon, F. M., Baud, B., Habing, H. J., de Jong, T., Harris, S., and Pottasch, S. R. 1984, *Ap. J. (Letters)*, **278**, L41.
Olnon, F. M., Walterbos, R. A. M., Habing, H. J., Matthews, H. E., Winnberg, A., Brezinska, H., and Baud, B. 1981, *Ap. J. (Letters)*, **245**, L103.
Paczyński, B. 1970, *Acta Astr.*, **20**, 47.
Werner, M. W., Beckwith, S., Gatley, I., Sellgren, K., and Berriman, G. 1980, *Ap. J.*, **239**, 540.

B. Baud: Department of Space Research, University of Groningen, P.O. Box 800, 9700 AV Groningen, The Netherlands

A. F. Bentley: Department of Natural Sciences, Eastern Montana College, Billings, MT 59101

A. I. Sargent: Owens Valley Radio Observatory, California Institute of Technology 320-47, Pasadena, CA 91125

M. W. Werner: NASA-Ames Research Center, MS 245-6, Moffett Field, CA 94305